Convergence analysis of inertial lift force estimates using the finite element method

Brendan Harding[1]

March 7, 2019

Abstract

We conduct a convergence analysis for the estimation of inertial lift force on a spherical particle suspended in flow through a straight square duct using the finite element method. Specifically we consider the convergence of an inertial lift force approximation with respect to a range of factors including the truncation of the domain, the resolution of the tetrahedral mesh and the boundary conditions imposed at the (truncated) ends of the domain. Additionally, we compare inertial lift estimations obtained via a variant of the Lorentz reciprocal theorem with those obtained via those obtained via a direct integration of fluid stresses over the particle surface.

Contents

1 Introduction

Inertial lift force is a phenomena in which particles/cells suspended in fluid flow through micro-scale devices experience a small forces that perturbs their motion from fluid streamlines. This is exploited in range of medical technologies including the separation and identification of circulating tumour cells [13]. Inertial lift has been studied analytically for simple flows bounded

by two walls over many decades, see for example [7, 12, 2], but for flows in devices of practical interest it is generally necessary to compute estimates of the inertial lift force.

Many methods for estimating the inertial lift force on a particle have been developed and investigated in the literature including, but not limited to, immersed boundary finite difference methods [10], direct forcing fictitious domain methods [14, 11], spectral methods [15], and finite element methods [3]. Typically these methods are used in studies which solve the full Navier–Stokes equations over a range of Reynolds numbers. We are interested in the estimation of the inertial lift force via a perturbation expansion of the Navier–Stokes equations with respect to the particle Reynolds number and with the use of a variant of the Lorentz reciprocal theorem, as described in [9]. Whilst our research has focused on the migration of particles within curved duct flows [5, 6], in this short paper we examine the simpler case of straight square duct flow noting that much of what is discussed is transferable to curved duct geometries.

We examine various aspects affecting the convergence of the inertial lift force when approximated via the solution of several Stokes equations with the finite element method. Section 2 provides a brief account of how the inertial lift force is estimated. A more detailed derivation and explanation may be found in [9], only parts essential to this paper are repeated in this section. In Section 3 we then provide and discuss the results of a convergence analysis for the finite element code which has been developed within the open source computing platform FEniCS [1]. Lastly, we summarise our findings and discuss aspects of the computation that could be improved.

2 Background

Suppose ℓ denotes the side length of the square cross-section, then, without loss of generality, we may take the duct interior to be $\mathcal{D} = \{\boldsymbol{x} = (x, y, z) \in \mathbb{R}^3 : x, y \in [-\ell/2, \ell/2]\}$. A fluid, with density ρ and viscosity μ, is pumped through the duct via a (constant) pressure gradient to produce a laminar Poiseuille flow. A solid/rigid spherical particle with radius a and neutral buoyancy (i.e. density ρ) is then suspended in the flow through the duct. The location of its centre is denoted as $\boldsymbol{x}_p = (x_p, y_p, z_p)$. Necessarily one has $x_p, y_p \in [-\ell/2 + a, \ell/2 - a)]$ and, without loss of generality, we may assume $z_p = 0$ (at $t = 0$). The setup is depicted in Figure 1. The fluid domain is then $\mathcal{F} = \{\boldsymbol{x} \in \mathcal{D} : \|\boldsymbol{x} - \boldsymbol{x}_p\|_2 \geq a\}$. The particle is taken to have a velocity $\boldsymbol{u}_p = (u_p, v_p, w_p)$ such that $u_p = v_p = 0$ and $w_p = \partial z_p/\partial t$ is constant. Additionally, the particle is free to spin about its centre with

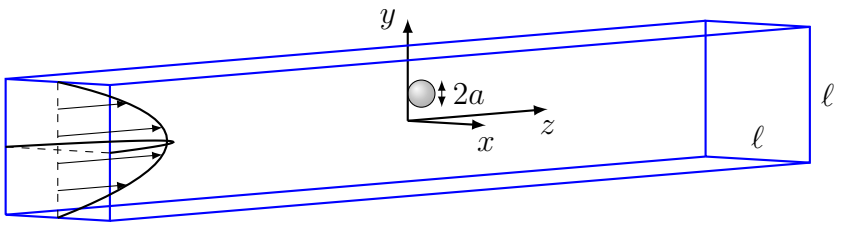

Figure 1: The setup of the duct.

(constant) angular velocity $\boldsymbol{\Omega}_p$ with z component taken to be zero.

It is convenient to work in a frame of reference that is translating in the z direction so that the particle location remains fixed. In this frame, the domain $\mathcal{F}$ remains static/fixed and, given $\boldsymbol{u}_p, \boldsymbol{\Omega}_p$ as described above, the system is steady. While we have assumed that $u_p = v_p = 0$, our goal is to estimate the hydrodynamic force on the particle in the x, y directions which would ultimately lead to a non-zero (albeit small) u_p, v_p.

It is useful to separate the fluid flow into the background flow $\bar{p}, \bar{\boldsymbol{u}}$ (defined on $\mathcal{D}$), which denotes the steady laminar flow in the absence of a particle, and the disturbance flow $q, \boldsymbol{v}$ (defined on $\mathcal{F}$), which is the change in background flow caused by the presence of the particle. The background flow has pressure $\bar{p} = -Pz$, for some constant $P > 0$, and velocity $\bar{\boldsymbol{u}}$ satisfying $\nabla^2 \bar{\boldsymbol{u}} = -(P/\mu)\boldsymbol{e}_z$ with the boundary conditions $\bar{\boldsymbol{u}} = \boldsymbol{0}$ on $\partial\mathcal{D}$. With $\bar{\boldsymbol{u}} = (\bar{u}, \bar{v}, \bar{w})$ it is straightforward to show that $\bar{u} = \bar{v} = 0$ and

$$\bar{w} = \frac{P}{\mu} \sum_{k=0}^{\infty} \frac{4\ell^2(-1)^k}{\pi^3(2k+1)^3} \cos((2k+1)\pi x/\ell) \left(1 - \frac{\cosh((2k+1)\pi y/\ell)}{\cosh((2k+1)\pi/2)}\right).$$

While the fluid motion, in the presence of a particle, is assumed to be modelled by the Navier–Stokes equations we make use of a perturbation expansion in the (particle) Reynolds number so that one need only solve a few Stokes' problems to approximate the inertial lift force. For convenience we define the functionals $\mathcal{P}(\boldsymbol{f}, \boldsymbol{b}), \boldsymbol{\mathcal{U}}(\boldsymbol{f}, \boldsymbol{b})$ which, given the vector fields $\boldsymbol{f}, \boldsymbol{b}$ defined on the fluid domain $\mathcal{F}$ and particle surface $\partial(\mathcal{D}\backslash\mathcal{F})$ respectively, return the pressure and velocity fields that satisfy

$$\nabla \cdot (-\mathcal{P}(\boldsymbol{f}, \boldsymbol{b})\mathbb{I} + \mu\,(\nabla\boldsymbol{\mathcal{U}}(\boldsymbol{f}, \boldsymbol{b}) + \nabla\boldsymbol{\mathcal{U}}(\boldsymbol{f}, \boldsymbol{b})^{\mathsf{T}})) = \boldsymbol{f} \quad \text{on } \mathcal{F}\,, \tag{1a}$$

$$\nabla \cdot \boldsymbol{\mathcal{U}}(\boldsymbol{f}, \boldsymbol{b}) = 0 \quad \text{on } \mathcal{F}\,, \tag{1b}$$

$$\boldsymbol{\mathcal{U}}(\boldsymbol{f}, \boldsymbol{b}) = \boldsymbol{0} \quad \text{on } \partial\mathcal{D}\,, \tag{1c}$$

$$\boldsymbol{\mathcal{U}}(\boldsymbol{f}, \boldsymbol{b}) = \boldsymbol{b} \quad \text{on } \partial(\mathcal{D}\backslash\mathcal{F})\,, \tag{1d}$$

where $\mathbb{I}$ is the identity tensor. Lastly, given a flow $p, \boldsymbol{u}$ on $\mathcal{F}$, the hydrody-

namic force and torque on the particle is given by

$$\boldsymbol{F}(p,\boldsymbol{u}) = \int_{|\boldsymbol{x}-\boldsymbol{x}_p|=a} \boldsymbol{n}\cdot(-p\mathbb{I}+\mu(\nabla\boldsymbol{u}+\nabla\boldsymbol{u}^\intercal))\,dS\,,$$
$$\boldsymbol{T}(p,\boldsymbol{u}) = \int_{|\boldsymbol{x}-\boldsymbol{x}_p|=a} (\boldsymbol{x}-\boldsymbol{x}_p)\times(\boldsymbol{n}\cdot(-p\mathbb{I}+\mu(\nabla\boldsymbol{u}+\nabla\boldsymbol{u}^\intercal)))\,dS\,,$$

where the normal $\boldsymbol{n}$ is taken to be outward pointing from the particle centre.

We are now equipped to describe the process of estimating the inertial lift force. The following description is given in the dimensional setting but is straightforward to non-dimensionalise (with length scale a, velocity scale Ua/ℓ and pressure scale $\mu U/\ell$, where $U := \bar{w}(\boldsymbol{0})$, such that the inertial terms of the Navier–Stokes equations are found to scale with the particle Reynolds number $\mathrm{Re}_p = (\rho/\mu)Ua^2/\ell$). First one needs to solve the leading order approximation of the disturbance flow. Specifically, this is given by

$$q_0,\boldsymbol{v}_0 := \mathcal{P}(\boldsymbol{0},-\bar{\boldsymbol{u}}+\boldsymbol{u}_p+\boldsymbol{\Omega}_p\times(\boldsymbol{x}-\boldsymbol{x}_p)),\boldsymbol{\mathcal{U}}(\boldsymbol{0},-\bar{\boldsymbol{u}}+\boldsymbol{u}_p+\boldsymbol{\Omega}_p\times(\boldsymbol{x}-\boldsymbol{x}_p))\,,$$

with the particle velocity and spin such that the system is in equilibrium, that is $\boldsymbol{F}(q_0,\boldsymbol{v}_0)=\boldsymbol{T}(q_0,\boldsymbol{v}_0)=\boldsymbol{0}$. Given the linearity of Stokes' equation, and some components of $u_p,\boldsymbol{\Omega}_p$ being zero, this can be solved by:

1. First solving each of

$$\begin{aligned}
&q_{0,1},\boldsymbol{v}_{0,1} = \mathcal{P}(\boldsymbol{0},\boldsymbol{e}_z),\boldsymbol{\mathcal{U}}(\boldsymbol{0},\boldsymbol{e}_z)\,,\\
&q_{0,2},\boldsymbol{v}_{0,2} = \mathcal{P}(\boldsymbol{0},\boldsymbol{e}_x\times(\boldsymbol{x}-\boldsymbol{x}_p)),\boldsymbol{\mathcal{U}}(\boldsymbol{0},\boldsymbol{e}_x\times(\boldsymbol{x}-\boldsymbol{x}_p))\,,\\
&q_{0,3},\boldsymbol{v}_{0,3} = \mathcal{P}(\boldsymbol{0},\boldsymbol{e}_y\times(\boldsymbol{x}-\boldsymbol{x}_p)),\boldsymbol{\mathcal{U}}(\boldsymbol{0},\boldsymbol{e}_y\times(\boldsymbol{x}-\boldsymbol{x}_p))\,,\\
&q_{0,4},\boldsymbol{v}_{0,4} = \mathcal{P}(\boldsymbol{0},\bar{\boldsymbol{u}}),\boldsymbol{\mathcal{U}}(\boldsymbol{0},\bar{\boldsymbol{u}})\,.
\end{aligned}$$

2. Then compute $\boldsymbol{F}_k = \boldsymbol{F}(q_{0,k},\boldsymbol{v}_{0,k})$ and $\boldsymbol{T}_k = \boldsymbol{T}(q_{0,k},\boldsymbol{v}_{0,k})$ for $k=1,2,3,4$ and solve the linear system

$$(w_p\boldsymbol{F}_1+\Omega_{p,x}\boldsymbol{F}_2+\Omega_{p,y}\boldsymbol{F}_3-\boldsymbol{F}_4)\cdot\boldsymbol{e}_z = 0\,, \tag{2a}$$
$$(w_p\boldsymbol{T}_1+\Omega_{p,x}\boldsymbol{T}_2+\Omega_{p,y}\boldsymbol{T}_3-\boldsymbol{T}_4)\cdot\boldsymbol{e}_x = 0\,, \tag{2b}$$
$$(w_p\boldsymbol{T}_1+\Omega_{p,x}\boldsymbol{T}_2+\Omega_{p,y}\boldsymbol{T}_3-\boldsymbol{T}_4)\cdot\boldsymbol{e}_y = 0\,, \tag{2c}$$

   where $\boldsymbol{\Omega}_p = (\Omega_{p,x},\Omega_{p,y},\Omega_{p,z})$ (recalling $\boldsymbol{u}_p=(0,0,w_p)$ and $\Omega_{p,z}=0$).

3. Set $(q_0,\boldsymbol{v}_0) = w_p(q_{0,1},\boldsymbol{v}_{0,1})+\Omega_{p,y}(q_{0,2},\boldsymbol{v}_{0,2})+\Omega_{p,y}(q_{0,3},\boldsymbol{v}_{0,3})-(q_{0,4},\boldsymbol{v}_{0,4})$.

The inertial lift force can now be computed by solving for the first correction to the leading order disturbance. Specifically, let

$$\boldsymbol{f}_1 = \rho\big((\boldsymbol{v}_0+\bar{\boldsymbol{u}}-w_p\boldsymbol{e}_z)\cdot\nabla\boldsymbol{v}_0+\boldsymbol{v}_0\cdot\nabla\bar{\boldsymbol{u}}\big)\,, \tag{3}$$

then the first correction for the disturbance is given by

$$q_1, \boldsymbol{v}_1 := \mathcal{P}(\boldsymbol{f}_1, \boldsymbol{0}), \boldsymbol{\mathcal{U}}(\boldsymbol{f}_1, \boldsymbol{0})\,.$$

The inertial lift force can then be computed directly as $\boldsymbol{F}(q_1, \boldsymbol{v}_1)$ (noting it is the x, y components that are of principal interest). Note in equation (3) we include the $-w_p \boldsymbol{e}_z \cdot \nabla \boldsymbol{v}_0$ which is absent in [9] but can be found in [8].

However, rather than this direct approach, the inertial lift force can be obtained without needing to explicitly solve for $q_1, \boldsymbol{v}_1$. In particular, let $\hat{\boldsymbol{u}}_x := \boldsymbol{\mathcal{U}}(\boldsymbol{0}, \boldsymbol{e}_x)$ and $\hat{\boldsymbol{u}}_y := \boldsymbol{\mathcal{U}}(\boldsymbol{0}, \boldsymbol{e}_y)$, then a variant of the Lorentz reciprocal theorem can be used to show that

$$\boldsymbol{e}_x \cdot \boldsymbol{F}(q_1, \boldsymbol{v}_1) = -\int_{\mathcal{F}} \hat{\boldsymbol{u}}_x \cdot \boldsymbol{f}_1 \, dV\,, \quad \text{and} \quad \boldsymbol{e}_y \cdot \boldsymbol{F}(q_1, \boldsymbol{v}_1) = -\int_{\mathcal{F}} \hat{\boldsymbol{u}}_y \cdot \boldsymbol{f}_1 \, dV\,. \tag{4}$$

Again we refer the reader to [9] for further details.

This second approach may appear to be more effort since two Stokes' problems need to be solved (i.e. to find $\hat{\boldsymbol{u}}_x, \hat{\boldsymbol{u}}_y$) as opposed to one (for $q_1, \boldsymbol{v}_1$). However, it is important to realise that one may want to compute $\hat{\boldsymbol{u}}_x, \hat{\boldsymbol{u}}_y$ (and the corresponding pressure fields $\hat{p}_x, \hat{p}_y$) regardless in order to estimate the drag coefficients on the particle in the respective directions. For instance, these can then be used to determine the terminal lateral velocity a particle may achieve as a result of the inertial lift force. In this context, the application of the Lorentz reciprocal theorem then provides a computational saving. Furthermore, whilst beyond the scope of this paper, it is a far more convenient form to use for further analysis since linear expansions of $\boldsymbol{v}_0$ can be substituted into equation (3) and subsequently (4) to obtain a wealth of additional information about the inertial lift force at very little cost. Lastly, the results that follow demonstrate the computation of inertial lift force via the Lorentz reciprocal theorem is typically more accurate than the direct estimate (from explicitly calculating $\boldsymbol{F}(q_1 \boldsymbol{v}_1)$).

3 Results

The finite element method was implemented within the open source computing platform FEniCS [1]. Our implementation uses the standard weak formulation of Stokes' equations (1). The domain is truncated in the z direction and two different boundary conditions are considered at the truncated ends, the 'natural' boundary condition which enforces zero normal stress, and the 'zero' boundary condition which enforces no-slip and no-penetration. In the latter case, the $\nabla \boldsymbol{\mathcal{U}}^{\intercal}$ components can be dropped from the weak formulation whereas they must remain in the case of 'natural' boundary conditions.

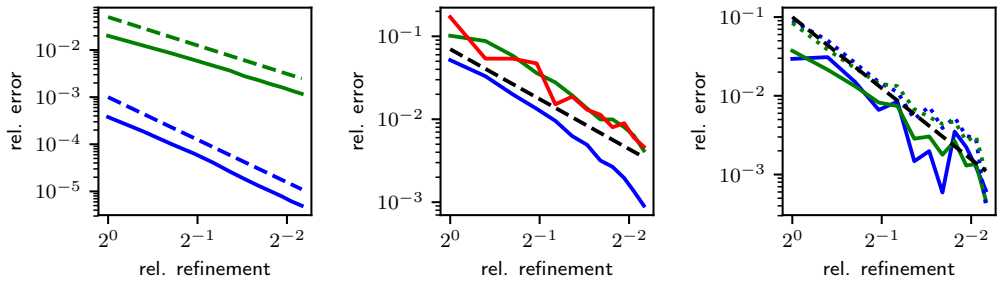

(a) (b) (c)

Figure 2: Plots showing the convergence in: (a) the leading order disturbance flow solution $q_0, \boldsymbol{v}_0$, (b) representative force and torque coefficients that determine the spin and velocity of the particle, and (c) the x, y components of the inertial lift force on the particle. See text for further details.

Tetrahedral meshes of the (truncated) domain were generated using the gmsh software [4]. The resolution is generally made to be much coarser far from the particle since the disturbance flow is expected to decay away from the particle. This is a particular computational advantage from formulating the problem in terms of the disturbance flow. Standard Taylor-Hood elements were used, that is first/second order Lagrange elements were used for the pressure/velocity spaces respectively. The minres algorithm was used to solve the resulting linear system using an algebraic multi-grid preconditioner based on the mass matrix. In order to estimate the error in the solution (for a given mesh resolution) the same problem was solved using second/third order Lagrange elements for pressure/velocity respectively. The solution from the lower order space is then projected into the higher order space so that the difference between the two can be computed.

All computations in this section consist of a particle with radius $a = 0.2$ located at $\boldsymbol{x}_p = (0.2, 0.4, 0.0)$ within a duct having side length $\ell = 2$. The duct is truncated at a distance 4ℓ either side of the particle (i.e. with total length $8\ell = 16$) except where convergence with respect to domain length is considered. Each mesh is non-uniform with surface elements whose edges approximately five times smaller on the particle boundary compared to at the two ends of the duct. The relative degree of refinement, denoted here as h, is taken to be the ratio of the cube root of the average cell volume compared to those in the coarsest mesh (consisting of $\approx 19,000$ tetrahedra compared to the finest mesh which has $\approx 1,600,000$ tetrahedra).

We begin by examining mesh convergence with 'zero' boundary conditions at the ends of the duct (results were found to be similar for 'natural' boundary

conditions and are omitted). Figure 2(a) shows the relative convergence in the $q_0, \boldsymbol{v}_0$ solution, specifically it is the 2-norm of the difference between solutions computed in both the low and high order function spaces on each mesh. It is clear that convergence in $q_0, \boldsymbol{v}_0$ is approximately 2nd and 3rd order respectively, as is expected for linear and quadratic elements. Of particular interest is $\boldsymbol{v}_0$, since this plays a significant role in the estimation of the inertial lift force via the reciprocal equation (4), and it is clear that this is reasonably accurate, even on the coarsest mesh.

Figure 2(b) shows the relative convergence of each of $\boldsymbol{F}_4 \cdot \boldsymbol{e}_z, \boldsymbol{T}_4 \cdot \boldsymbol{e}_x, \boldsymbol{T}_4 \cdot \boldsymbol{e}_y$ in blue, green and red respectively. These are representative of the coefficients that are used to determine the velocity and spin of the particle in equation (2). Because these depend on the pressure it is reasonable to expect h^2 convergence, as indicated by the dashed black line, and the results seem consistent with this, if not slightly better.

Figure 2(c) shows the relative convergence of the x, y components of the inertial lift force in blue and green respectively. The solid lines are the results of the reciprocal calculation whilst the dotted lines are from the direct approach. The dashed black line shows the slope of h^3 and seems to be a reasonable fit. This is somewhat surprising because of the dependence of the inertial lift on the gradient of the velocity field (and also pressure in the case of the direct calculation) which would lead one to expect convergence at the rate h^2. Note that the reciprocal result is generally more accurate than the direct result. The error is less than 1% for meshes with approximately $150,000$ tetrahedra or more. There is some noise in the reciprocal result on the finer meshes which we expect is due to the finite accuracy of our best guess at the true inertial lift force.

The main difference due to the different choice of boundary conditions was observed in examining convergence with respect to duct length. In particular, the drag coefficient in the z direction is especially affected. In the case of 'natural' boundary conditions the solution $\boldsymbol{\mathcal{U}}(\boldsymbol{0}, \boldsymbol{e}_z)$ does not completely decay far away from the particle since the imposed motion of the particle drags a small volume of liquid through the duct with it. In contrast, this cannot be the case when no-slip/penetration is enforced at the ends of the duct, and ultimately results in a larger drag coefficient.

Figure 3(a) shows the relative convergence of each of $\boldsymbol{F}_4 \cdot \boldsymbol{e}_z, \boldsymbol{T}_4 \cdot \boldsymbol{e}_x, \boldsymbol{T}_4 \cdot \boldsymbol{e}_y$ in blue, green and red respectively with respect to the length of the duct in the case of 'natural' boundary conditions. Note that the (local) mesh resolution was not changed as the duct length was increased, i.e. so that longer ducts contained more tetrahedra and the convergence seen primarily reflects the length of the duct. Interestingly, we observed that since both $\boldsymbol{F}_1 \cdot \boldsymbol{e}_z$ and $\boldsymbol{F}_4 \cdot \boldsymbol{e}_z$ are effected in a similar way, the resulting particle velocity w_p obtained

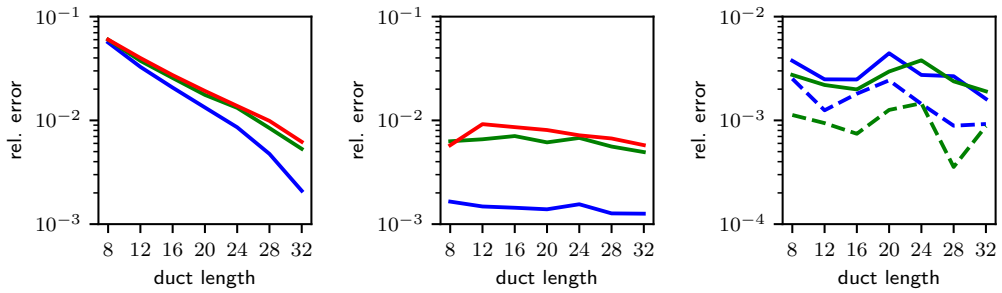

(a) (b) (c)

Figure 3: Plots showing differences in convergence with respect to the duct length for: (a) drag and torque coefficients in the case of 'natural' boundary conditions, (b) drag and torque coefficients in the case of 'zero' boundary conditions, and (c) inertial lift force estimates in the case of 'zero' boundary conditions. See text for details.

via equation (2) is quite accurate independent of the duct length (up to mesh convergence error).

In contrast, Figure 3(b) shows virtually no convergence in the same coefficients when 'zero' boundary conditions are applied. Notice the results are more accurate to begin with and are essentially already converged up to the given level of refinement for the mesh. Furthermore, we find that the resulting particle velocity and inertial lift coefficients do not differ significantly. This is evident in Figure 3(c) which shows the x, y components of the inertial lift force in blue and green respectively with solid lines denoting the result of the reciprocal calculation while the dotted lines show the result of the direct calculation. The results demonstrate degree of convergence remains similar independent of duct length (and essentially reflect the degree of mesh convergence). This suggests a duct length even shorter than 8 could perhaps be used in the case of 'zero' boundary conditions with minimal loss of accuracy.

4 Conclusions

We have examined the convergence of a finite element code for estimating inertial lift forces with respect to mesh resolution, duct length and boundary conditions. From these results we conclude that imposing 'zero' boundary conditions on the ends and using the reciprocal equation to estimate the inertial lift force seems to be the most robust approach. Going forward we would like to further optimise the local size/distribution of tetrahedra over the domain, potentially via an analysis of the adjoint problem. The use of

periodic boundary conditions at the ends could also be considered. Lastly, an evaluation of the validity of the perturbation approximation to the inertial lift force, i.e. in comparison with full Navier–Stokes solutions over a suitable range of Re_p, would also be valuable.

Acknowledgements Computations were carried out using supercomputing resources provided by the Phoenix HPC service at the University of Adelaide. This research was supported under Australian Research Council's Discovery Projects funding scheme (project number DP160102021).

References

[1] M.S. Alnæs et al. "The FEniCS Project Version 1.5". In: *Archive of Numerical Software* 3.100 (2015), pp. 9–23. DOI: 10.11588/ans.2015.100.20553 (cit. on pp. 2, 5).

[2] E. S. Asmolov. "The inertial lift on a spherical particle in a plane Poiseuille flow at large channel Reynolds number". In: *Journal of Fluid Mechanics* 381 (1999), pp. 63–87. DOI: 10.1017/S0022112098003474 (cit. on p. 2).

[3] D. Di Carlo. "Inertial microfluidics". In: *Lab Chip* 9 (21 2009), pp. 3038–3046. DOI: 10.1039/B912547G (cit. on p. 2).

[4] C. Geuzaine and J.-F. Remacle. "Gmsh: A 3-D finite element mesh generator with built-in pre- and post-processing facilities". In: *International Journal for Numerical Methods in Engineering* 79.11 (2009), pp. 1309–1331. DOI: 10.1002/nme.2579 (cit. on p. 6).

[5] B. Harding. "A study of inertial particle focusing in curved microfluidic ducts with large bend radius and low flow rate". In: *Proceedings of 21st Australasian Fluid Mechanics Conference*. 603. 2018 (cit. on p. 2).

[6] B. Harding, Y. M. Stokes, and A. L. Bertozzi. "Effect of inertial lift on a spherical particle suspended in flow through a curved duct". In: *Journal of Fluid Mechanics* (in review). (arXiv preprint: 1902.06848) (cit. on p. 2).

[7] B. P. Ho and L. G. Leal. "Inertial migration of rigid spheres in two-dimensional unidirectional flows". In: *Journal of Fluid Mechanics* 65.2 (1974), pp. 365–400. DOI: 10.1017/S0022112074001431 (cit. on p. 2).

[8] A. J. Hogg. "The inertial migration of non-neutrally buoyant spherical particles in two-dimensional shear flows". In: *Journal of Fluid Mechanics* 272 (1994), pp. 285–318. DOI: 10.1017/S0022112094004477 (cit. on p. 5).

[9] K. Hood, S. Lee, and M. Roper. "Inertial migration of a rigid sphere in three-dimensional Poiseuille flow". In: *Journal of Fluid Mechanics* 765 (2015), pp. 452–479. DOI: 10.1017/jfm.2014.739 (cit. on pp. 2, 5).

[10] N. Nakagawa et al. "Inertial migration of a spherical particle in laminar square channel flows from low to high Reynolds numbers". In: *Journal of Fluid Mechanics* 779 (2015), pp. 776–793. DOI: 10.1017/jfm.2015.456 (cit. on p. 2).

[11] T.-W. Pan and R. Glowinski. "Direct simulation of the motion of neutrally buoyant balls in a three-dimensional Poiseuille flow". In: *Comptes Rendus Mcanique* 333.12 (2005). Fluid-solid interactions: modeling, simulation, bio-mechanical applications, pp. 884–895. DOI: 10.1016/j.crme.2005.10.006 (cit. on p. 2).

[12] J. A. Schonberg and E. J. Hinch. "Inertial migration of a sphere in Poiseuille flow". In: *Journal of Fluid Mechanics* 203 (1989), pp. 517–524. DOI: 10.1017/S0022112089001564 (cit. on p. 2).

[13] M. E. Warkiani et al. "Slanted spiral microfluidics for the ultra-fast, label-free isolation of circulating tumor cells". In: *Lab Chip* 14 (1 2014), pp. 128–137. DOI: 10.1039/C3LC50617G (cit. on p. 1).

[14] B. H. Yang et al. "Migration of a sphere in tube flow". In: *Journal of Fluid Mechanics* 540 (2005), pp. 109–131. DOI: 10.1017/S0022112005005677 (cit. on p. 2).

[15] L. Zeng, S. Balachandar, and P. Fischer. "Wall-induced forces on a rigid sphere at finite Reynolds number". In: *Journal of Fluid Mechanics* 536 (2005), pp. 1–25. DOI: 10.1017/S0022112005004738 (cit. on p. 2).

Author address

1. **Brendan Harding**, School of Mathematical Sciences, The University of Adelaide, South Australia 5005, AUSTRALIA.
mailto:brendan.harding@adelaide.edu.au
orcid:0000-0002-6755-9998